LANGMUIR

Article

pubs.acs.org/Langmuir

Interplay between Intrinsic Conformational Propensities and Intermolecular Interactions in the Self-Assembly of Short Surfactant-like Peptides Composed of Leucine/Isoleucine

Peng Zhou,[†] Li Deng,[†] Yanting Wang,*[,‡] Jian R. Lu,*[,§] and Hai Xu*[,†]

[†]State Key Laboratory of Heavy Oil Processing and Centre for Bioengineering and Biotechnology, China University of Petroleum (East China), 66 Changjiang West Road, Qingdao, China

[‡]Institute of Theoretical Physics, Chinese Academy of Sciences, 55 East Zhongguancun Road, Beijing, China

[§]Biological Physics Laboratory, School of Physics and Astronomy, The University of Manchester Institution, Manchester M13 9PL, United Kingdom

Supporting Information

ABSTRACT: To study how the conformational propensities of individual amino acid residues, primary structures (i.e., adjacent residues and molecular lengths), and intermolecular interactions of peptides affect their self-assembly properties, we report the use of replica exchange molecular dynamics (REMD) to investigate the monomers, dimers, and trimers of a series of short surfactant-like peptides (I_3K, L_3K, L_4K, and L_5K). For four-residue peptides X_3K (I_3K and L_3K), the results show that their different aggregation behaviors arise from the different intrinsic conformational propensities of isoleucine and leucine. For L_mK peptides (L_3K, L_4K, and L_5K), the molecular length is found to dictate their aggregation via primarily modulating intermolecular interactions. Increasing the number of hydrophobic amino acid residues of L_mK peptides enhances their intermolecular H-bonding and promotes the formation of β-strands in dimer and trimer aggregates, overwhelming the intrinsic preference of Leu for helical structures. Thus, the interplay between the conformational propensities of individual amino acid residues for secondary structures and molecular interactions determines the self-assembly properties of the peptides, and the competition between intramolecular and intermolecular H-bonding interactions determines the probability of β-sheet alignment of peptide molecules. These results are validated by comparing simulated and experimental CD spectra of the peptides. This study will aid the design of short peptide amphiphiles and improve the mechanistic understanding of their self-assembly behavior.

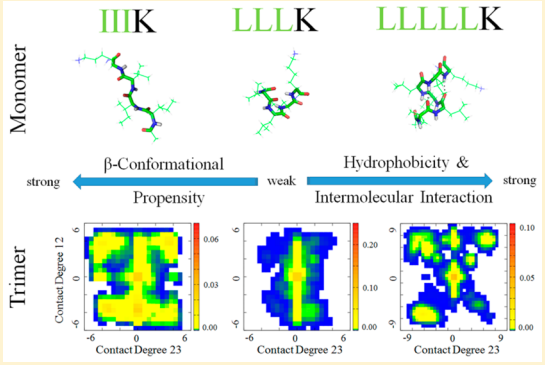

1. INTRODUCTION

The conformational propensities of amino acid residues for various secondary structures are important for peptide self-assembly because these features generally rule the self-assembling ability of peptide molecules and the shapes and sizes of the nanostructures formed.[1−4] Similar to folded proteins, even ultrashort peptides such as FF, IVD, and I_3K can form stable and well-defined secondary structures during self-assembly.[5−7] The adoption of secondary structures has been found to exert a substantial influence on the structures and properties of peptide aggregates.[7−10] In protein folding, various amino acid residues have been found to display their respective secondary structure propensities (SSPs),[11] which has been further consolidated with the development of bioinformatics.[12] To study and predict the secondary structures of amino acid sequences, many model molecules (e.g., Ac-X-NHMe, GX, XG, GXG, GGXGG, GGXA, and GGXAGG) have been studied by using the host−guest method in which the intrinsic conformational propensities of residues can be assessed.[13−15] The results from these studies usually vary, being dependent on which model system was chosen or which spectroscopic method was used.[16] Furthermore, the SSPs of residues in a sequence may be influenced by their adjacent amino acid residues.[13,17] To study this effect, a dipeptide system has been investigated by both experiments and simulations.[13,18] However, the dipeptides were found to have structures similar to denatured and natively unfolded proteins,[13] which gives few clues to the SSPs of folded proteins or self-assembling peptides.

Both the amino acid sequence and the environment have been found to affect the amino acid preference for secondary structures.[19] For example, Zhong et al. have shown that three amino acid sequences expected to be α-helical adopted primarily β-strands in their respective proteins.[19] For peptide self-assembly systems, there are a variety of intermolecular interactions that drive peptides to form various supramolecular

Received: January 25, 2016
Revised: April 15, 2016
Published: April 18, 2016

DOI: 10.1021/acs.langmuir.6b00287
Langmuir 2016, 32, 4662−4672

nanostructures.[1,20,21] During self-assembly, some peptides have shown completely different conformational propensities from the ones predicted according to protein folding. Typical examples are LKLKLKL and L_5K, which can undergo self-assembly to form well-ordered aggregates by taking β-sheet structures, although Leu is widely perceived to have a strong propensity for α-helical structures.[22,23] These results imply that intermolecular interactions may have a remarkable impact on the conformational propensities of amino acid residues in peptide self-assembly.

Although a considerable number of self-assembling peptides have so far been found from nature or de novo designed, documented studies have mainly focused on their self-assembled nanostructures and potential applications.[1−10,23−27] On the other hand, the model peptides chosen for conformational propensity studies were seldom focused on their self-assembly properties.[13−15] Thus, there is currently a lack of investigation on the conformational propensities of the amino acid residues of self-assembling peptides and how they are affected by adjacent residues and intermolecular interactions. In fact, these microscopic factors are most likely to play a mechanistic role in determining the self-assembling ability of peptides and the self-assembled nanostructures and properties.

To microscopically investigate the conformational propensities and chain geometry of self-assembling peptides and correlate these properties with their self-assembly, we select a series of short peptides, i.e., I_3K, L_3K, L_4K, and L_5K. The first two have the same molecular weight and similar hydrophobicity but self-assemble into completely different nanostructures (nanofibrils versus spherical stacks).[23] β-Sheet structures were found to be dominant in the self-assembly of I_3K but absent in the self-assembly of L_3K, which is consistent with the intrinsic SSPs of Ile and Leu. However, with an increasing number of hydrophobic residues, we observed a structural transition, i.e., L_5K also self-assembled into nanofibrils with an evident β-sheet structure. We have proposed that such a structural transition arises from the increased intermolecular hydrophobic interactions, cooperatively enhancing the intermolecular H-bonding interactions of L_5K. These apparent differences and variations in the self-assembled nanostructures and the conformational propensities make the series of short peptides an ideal model set for our simulation study. In addition, the relatively short lengths of these peptides facilitate all-atom molecular dynamics simulations on them.

In this study, we employ the replica exchange molecular dynamics (REMD) technique to simulate the monomers, dimers, and trimers of the series of peptides I_3K, L_3K, L_4K, and L_5K. The dihedral angle (Φ, Ψ) distribution of residues, the chain geometry of peptide backbones, and the number of intramolecular and intermolecular H-bonds are carefully analyzed. We focus on the effects of intermolecular interactions in dimers and trimers and the length of hydrophobic chains on the above parameters. These correlations are proposed to ultimately determine the morphologies and diversity of self-assembled nanostructures. Such a mechanistic study is expected to enhance our understanding of the interplay between the conformational propensities of amino acid residues and intermolecular interactions as well as the competition between intramolecular and intermolecular H-bonding interactions.

2. METHODS

All-atom REMD simulations were performed with Gromacs 4.5.4.[28] A cubic simulation box with a side length of 3.0 nm was used for X_3K, 3.3 nm for L_4K, and 3.5 nm for L_5K in their monomer, dimer, and trimer simulations. The periodic boundary conditions were applied to the simulation boxes, and a cutoff of 1.0 nm was used for Lennard-Jones interactions. The neighbor list was updated for every step with a cutoff distance of 1.0 nm. The CharmM 27 all-atom force field and the TIP3P water model with a time step of 2 fs were used in our simulations.[29] The Lincs method was used to constrain all of the bond lengths to their equilibrium values. Electrostatic interactions were calculated using the particle mesh Ewald (PME) method with a cutoff distance in real space of 1.0 nm.[30] The peptides were initially randomly placed inside the simulation boxes. Before REMD simulations were run, the system was subjected to a 5000-step steepest-descent optimization to relax unfavorable contacts, followed by a 100 ps MD equilibration simulation with positional restraints applied to the peptide atoms. There were 32 replicas for each system running at temperatures of 280.0, 286.5, 293.2, 300.0, 306.9, 314.0, 321.3, 328.8, 336.4, 344.2, 352.2, 360.4, 368.8, 377.3, 386.1, 395.1, 404.2, 413.6, 423.2, 433.0, 443.1, 453.4, 463.9, 474.7, 485.7, 497.0, 508.5, 520.3, 532.4, 544.7, 557.4, and 570.3 K. The exchange interval was 200 steps (0.4 ps), and the configurations were dumped every 0.4 ps for further analysis. The exchange ratios were found to be 20−40% for X_3K, 20−35% for L_4K, and 17−33% for L_5K.

In terms of dihedral angle (Φ, Ψ) distributions in the Ramachandran map (Figure S1), the defined regions were α_R (denoted by H) $-122° \le \Phi \le -52°$ and $-84° \le \Psi \le -14°$, α_L (denoted by $\underline{H}$) $14° \le \Phi \le 84°$ and $52° \le \Psi \le 122°$, β (denoted by B) $-150° \le \Phi \le -70°$ and $95° \le \Psi \le 175°$, extended (PPII and near-β, denoted by E) $-180° \le \Phi \le -50°$ and $50° \le \Psi \le 180°$, $-180° \le \Phi \le -50°$ and $-180° \le \Psi \le -150°$, $0° \le \Phi \le 30°$ and $50° \le \Psi \le 180°$ (the β region is excluded from the extended region), and others (denoted by −). The end-to-end distance was analyzed by measuring the distance between the two chiral carbon atoms (C_α) of the residues at the termini. The contact degree was used to analyze the alignments of dimers and trimers, whose definitions have been given in our previous publication.[31] Note that when analyzing the trimer structures the order of the three peptide molecules was sorted dynamically to make the intermolecular distance between mass centers (D_{ij}, i, j = 1, 2, and 3) always follow the order $D_{12} < D_{23} < D_{13}$. Simulated circular dichroism (CD) spectra were calculated using the method developed by the Hirst group.[32,33]

Experimental CD spectra were recorded on a Biologic Mos-450/AF-CD spectrophotometer at room temperature (20 ± 2 °C) using a 0.1 mm quartz cell. The wavelength scans were performed between 190 and 260 nm with a 0.5 nm step. Each CD signal presented was the average of six independent sample measurements, expressed as $[\theta]$ (deg·cm^2·dmol^{-1}).

3. RESULTS AND DISCUSSION

3.1. Intrinsic Structural Propensities of X_3K Monomers. The REMD method has been widely adopted to study the structural distribution of molecules because it can efficiently sample free-energy basins by exchanging simulation replica running simultaneously at different temperatures.[31,34−37] We first apply this method to explore the intrinsic structural propensities of single X_3K molecules.

3.1.1. Dihedral Angle Distributions of Amino Acid Residues of X_3K Monomers. Dihedral angles (Φ, Ψ) are useful for quantifying the conformational preference of each amino

DOI: 10.1021/acs.langmuir.6b00287
Langmuir 2016, 32, 4662−4672

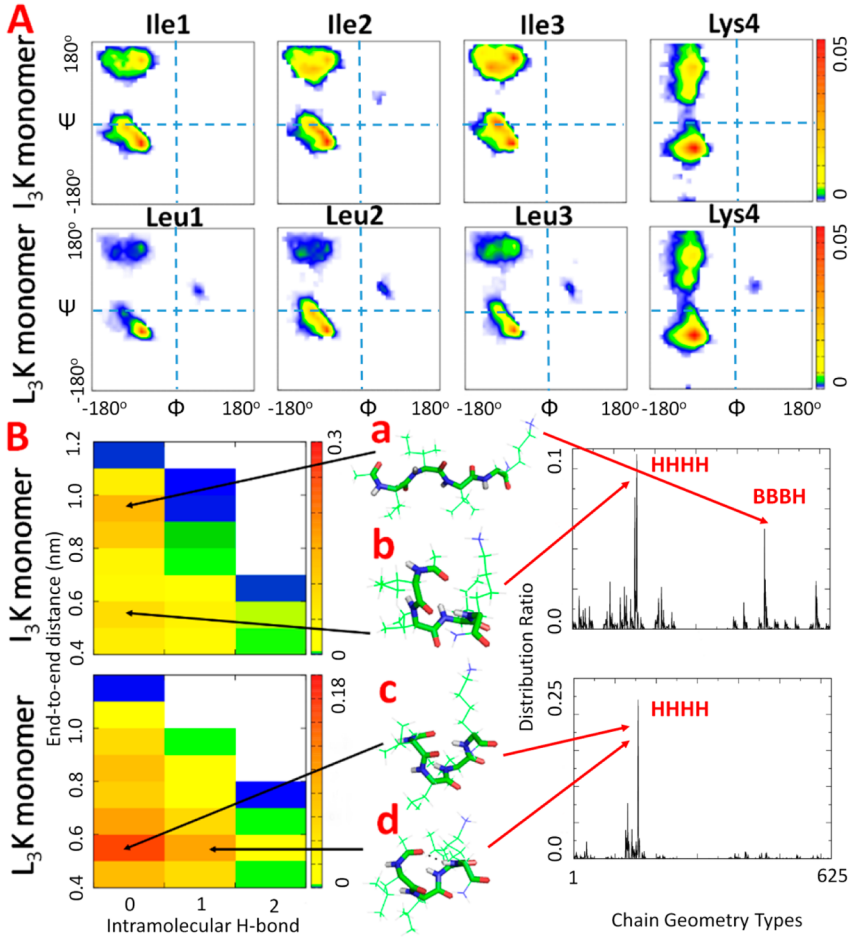

Figure 1. REMD simulation results of X_3K monomers. (A) Ramachandran maps for the residues of I_3K and L_3K in monomer simulations. (B) Left: Probability maps of the end-to-end distance and the intramolecular H-bond number of I_3K and L_3K monomers. Right: Chain geometry distributions of I_3K and L_3K monomers. The two main peaks for I_3K are HHHH and BBBH, and the highest peak for L_3K is HHHH. Four representative monomer structures (structures a–d) are given between the two panels in order to show intramolecular H-bonding.

acid residue in peptides for various secondary structures. As described in the Methods section and Figure S1, there are four typical residue conformations including α_R, α_L, β, and extended (PPII and near-β), which correspond to different (Φ, Ψ) regions in the Ramachandran map. As shown in Figure 1A, Ile residues of the I_3K monomer have two main dihedral angle regions that correspond to β/extended and α_R conformations. It is evident that Ile1 at the N-terminus has the lowest β/extended population, and the probability of Ile for β/extended conformations increases from the N-terminus to the C-terminus. Although Ile is usually perceived to have a stronger β/extended propensity than Lys, Ile1 and Lys4 at the two termini are found to have a similar (Φ, Ψ) distribution, leading to the likely formation of a similar microenvironment around Ile2 and Ile3. It is possible that because of the similar microenvironment the β/extended population of Ile2 is only slightly lower than that of Ile3.

Leu residues of the L_3K monomer have a minor (Φ, Ψ) region of α_L conformations, in addition to α_R and β/extended regions (Figure 1A). Similar to I_3K, Leu residues of L_3K also show an increased probability for β/extended conformations from the N-terminus to C-terminus. However, the β/extended population of each Leu residue of L_3K is clearly lower than that of the corresponding Ile of I_3K. Furthermore, Leu1 at the N-terminus has a much lower β/extended population than does Lys4 at the C-terminus, resulting in different microenvironments around Leu2 and Leu3 residues. As a result, the β/extended population of Leu2 is lower than that of Leu3 and close to that of Leu1.

To clarify the effect of adjacent residues, we then compare the (Φ, Ψ) distribution of X residues of the X_3K monomer with that of the GGXGG monomer. As shown in Figure S2, the Ile residue of GGIGG has a higher probability for β/extended conformations than does the Leu residue of GGLGG. This result is similar to the above results from I_3K and L_3K monomers and is also consistent with different intrinsic propensities of Ile and Leu for secondary structures. Furthermore, because of the effect of adjacent residues, Ile2 and Ile3 of I_3K show higher probabilities of taking β/extended conformations than does the Ile residue of GGIGG, and Leu1 and Leu2 residues of L_3K show stronger propensities for forming α_R conformations than does the Leu residue of GGLGG.

3.1.2. Structures of X_3K Monomers (Intramolecular H-Bonds and End-to-End Distances of X_3K Monomers). In the maps whose coordinates are the end-to-end distance and the intramolecular H-bond numbers (Figure 1B), the I_3K monomer is mainly concentrated in the extended state with an end-to-end distance of 0.9 nm, which does not contain intramolecular H-bonding. The end-to-end distance is defined as the distance

DOI: 10.1021/acs.langmuir.6b00287
Langmuir 2016, 32, 4662–4672

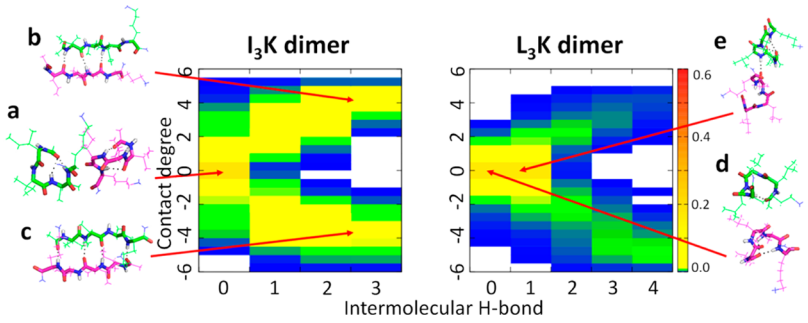

Figure 2. Probability maps of the contact degree and the intermolecular H-bond number of I_3K and L_3K in dimer simulations and representative intermolecular alignments. I_3K forms both antiparallel and parallel alignments with intermolecular H-bonding (structures b and c) and dimer aggregates with no intermolecular H-bonding but side-chain interactions only (structure a). L_3K tends to form coiled structures with intramolecular H-bonding (structures d and e), some of which can contact each other and form one intermolecular H-bond (structure e).

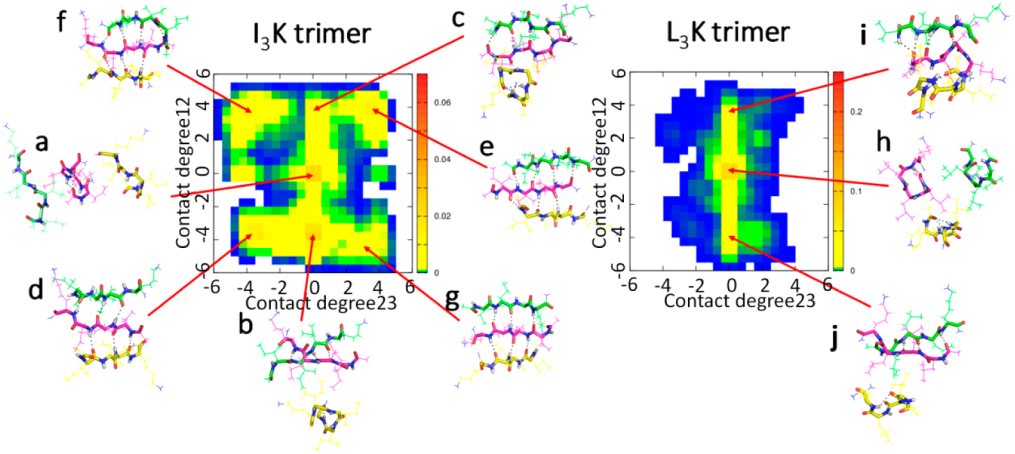

Figure 3. Probability maps of the contact degree of I_3K and L_3K in trimer simulations and representative intermolecular alignments. I_3K can form trimer aggregates with no intermolecular H-bonds (structure a), dimers with both antiparallel and parallel H-bonds (structures b and c), and trimers with antiparallel, parallel, and parallel/antiparallel mixed H-bonds (structures d–g). L_3K can form trimer aggregates without intermolecular H-bonds (structure h) and dimers with both parallel and antiparallel H-bonds (structures i and j) but no trimers with intermolecular H-bonds.

between the two chiral carbon atoms (C_α) at the N-terminus and the C-terminus, respectively, quantifying the degree of peptide backbone extension. For four-residue peptides, the extended state is defined as a monomer structure with an end-to-end distance equal to or above 0.8 nm, and the coiled state is defined below 0.7 nm. In the extended state, the representative I_3K monomer structure is shown as structure a in Figure 1B. The secondary populated state of the I_3K monomer is a coiled state that has an end-to-end distance of 0.5 nm and has no intramolecular H-bonding, such as structure b in Figure 1B. The L_3K monomer is mostly concentrated in a coiled state with an end-to-end distance of 0.5 nm and without intramolecular H-bonding, such as structure c in Figure 1B. In addition, the C═O of the acetyl group and the backbone N−H of the fourth residue (Lys4) can form one H-bond in its secondary populated state (structure d in Figure 1B).

Because the most populated coiled states of both I_3K and L_3K monomers have no intramolecular H-bonds, the driving force of X_3K monomers to form these coiled structures should arise from the hydrophobic interactions of amino acid side chains as well as the flexibility of peptide backbones. It is evident from monomer simulations that the backbone of I_3K is more rigid and harder to bend than that of L_3K.

The above results indicate that the structural difference between two short amphiphilic peptides with the same molecular weight and similar hydrophobicity arises from the conformational preferences of different hydrophobic residues for different secondary structures. To determine the relationship between the folded state (extended and coiled) of the whole molecule and the dihedral angle distribution of each amino acid residue, the chain geometry is then analyzed.

3.1.3. Chain Geometry Distributions of X_3K Monomers. The chain geometry is defined as the permutation of the conformations of all residues, which is able to show the whole backbone structure intuitively. As mentioned above, the conformation of each residue can be classified as α_R (H), α_L (H), β(B), extended (PPII and near-β) (E), or other (−) on the basis of its dihedral angle distribution (Figure S1). The permutation of a four-residue peptide has 5^4 (625) types of chain geometry. As shown in Figure 1B, although the sampling is drastically enhanced by the REMD technique, only limited ones out of all 625 types can be sampled.

Although the most populated chain geometry type (HHHH, 8.73%) belongs to the coiled state (Figure 1B), the I_3K monomer is observed to have more chain geometry types in the extended state, including BBBH (5.00%), BBBB (2.47%), EBBH (2.40%), −BBH (2.36%), HBBH (2.10%), and so on, as shown in Table S1 and Figure S3. In contrast, a much higher helical population (22.03%) of HHHH is observed for the L_3K monomer, and its chain geometry is more concentrated in the coiled states (Figure 1B, Table S1, and Figure S3).

DOI: 10.1021/acs.langmuir.6b00287
Langmuir 2016, 32, 4662–4672

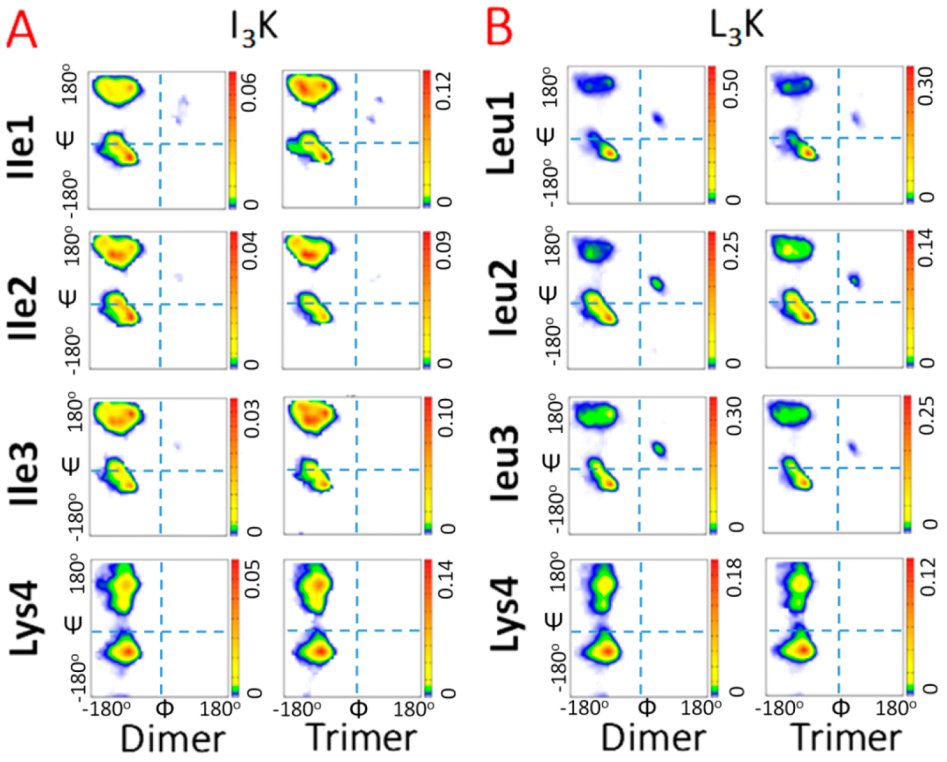

Figure 4. Ramachandran maps for the residues of (A) I_3K and (B) L_3K in dimer and trimer simulations.

3.2. Effects of Intermolecular Interactions on the Structural Propensities of X_3K Dimers and Trimers. *3.2.1. Structures of X_3K Dimers.* Dimer simulations are used to investigate the intermolecular alignment between monomers. The probability map is plotted with respect to the contact degree and the intermolecular H-bond number. The contact degree has been defined in our previous work,[31] which characterizes the proximity of C_α atoms between two peptide backbones and implies the possibility of interbackbone H-bonding. The REMD calculations show that the I_3K dimer can form both antiparallel and parallel alignments (Figure 2, structures b and c) as well as coiled structures (Figure 2, structure a). The degree of backbone contact is lower in the L_3K dimer than in the I_3K dimer (Figure 2). L_3K tends to form coiled structures with buried backbones, preventing further intermolecular H-bond formation (Figure 2, structure d). Additionally, the L_3K dimer can still form one intermolecular H-bond in the presence of intramolecular H-bonding, such as structure e in Figure 2.

3.2.2. Structures of X_3K Trimers. The trimers are then simulated to investigate further growth beyond dimers along the H-bonding direction. In I_3K trimer simulations, there are dimers with both antiparallel and parallel H-bonds (Figure 3, structures b and c); the parallel dimer can subsequently grow into a parallel trimer (Figure 3, structure e) or a parallel/antiparallel mixed trimer (Figure 3, structure f), and the antiparallel dimer can further form an antiparallel trimer (Figure 3, structure d) or an antiparallel/parallel mixed trimer (Figure 3, structure g). Note that structures f and g can be regarded as the same structure because they both have mixed alignments. These results suggest an aggregation pathway of I_3K molecules along the H-bonding direction. Similar to dimer simulations, there are a considerable number of I_3K trimer aggregates without intermolecular H-bonds (Figure 3, structure a). In L_3K trimer simulations, only dimers with intermolecular H-bonds are found (Figure 3, structures i and j), leaving a large population of trimer aggregates without intermolecular H-bonds (Figure 3, structure h). Similar to the case of L_3K dimer simulations, the domination of monomeric coiled structures disfavors the formation of intermolecular H-bonds and consequently their growth along the H-bonding direction.

3.2.3. Dihedral Angle Distributions of Residues in X_3K Dimers and Trimers. The above monomer simulations show that the intrinsic conformational propensity of each residue is closely related to its dihedral angle distribution and finally affects the folded state of monomers. Therefore, it is also required to know whether additional intermolecular interactions in aggregates can affect these properties of dimers and trimers. We compare the dihedral angle distributions of all residues in dimer and trimer simulations with those in monomer simulations. As shown in Figure 4A, all Ile residues in the I_3K dimer show an increased β/extended probability as a result of the packing of molecules along the H-bonding direction. In the I_3K trimer, Ile residues exhibit much higher β/extended populations. These results indicate that the propensity of Ile residues of I_3K for β/extended conformations can be strengthened as a result of intermolecular interactions. In L_3K dimer and trimer simulations, the probabilities of Leu2 and Leu3 for β/extended conformations also show a slightly increasing trend (Figure 4B), consistent with the formation of dimers with intermolecular H-bonds (structures i and j). Leu1 and Lys4 in dimer and trimer simulations retain β/extended populations similar to those in monomer simulations. In the case of L_3K, although intermolecular interactions do improve the probabilities of Leu2 and Leu3 to form β/extended conformations, such an improvement is not enough to stabilize the growth of L_3K trimer aggregates along the H-bonding direction.

DOI: 10.1021/acs.langmuir.6b00287
Langmuir 2016, 32, 4662−4672

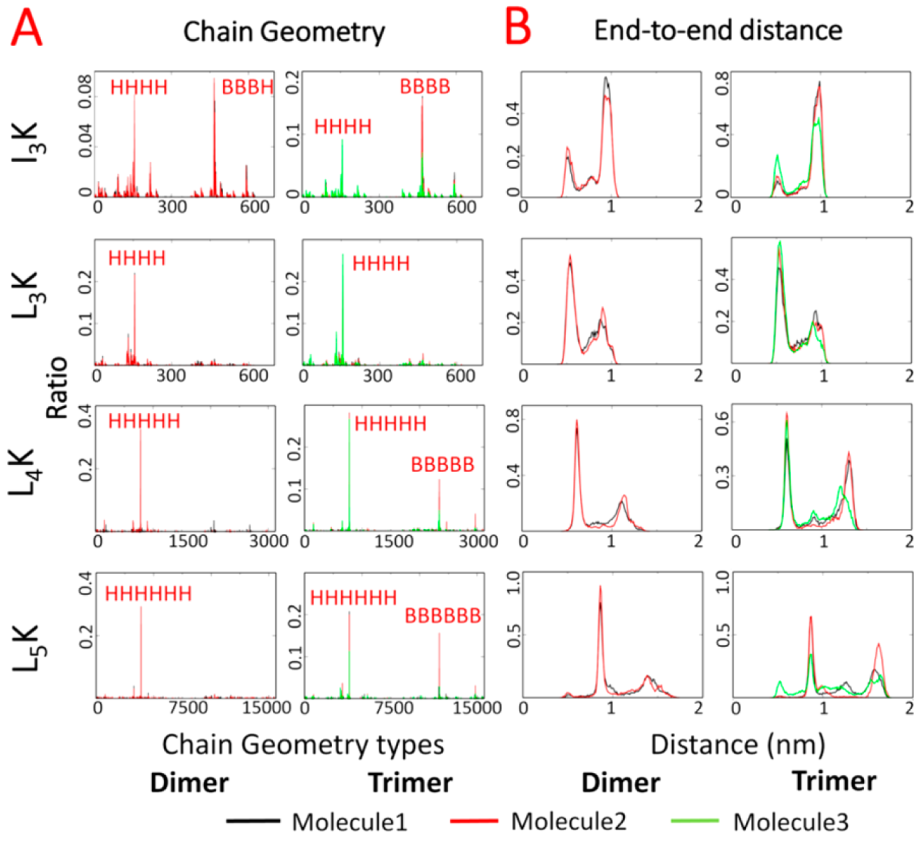

Figure 5. Chain geometry distributions and end-to-end distances of I_3K, L_3K, L_4K, and L_5K in dimer and trimer simulations.

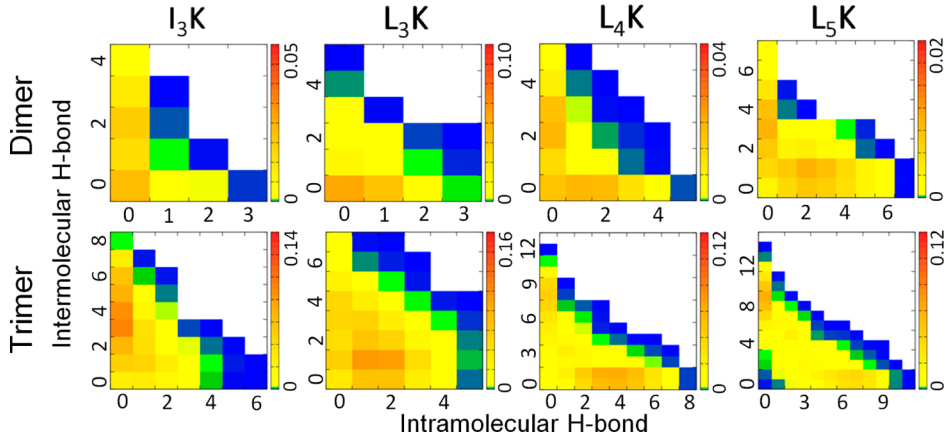

Figure 6. Probability maps of the numbers of inter- and intramolecular H-bonds of I_3K, L_3K, L_4K, and L_5K in dimer and trimer simulations.

3.2.4. Chain Geometry Distributions and End-to-End Distances of X_3K Dimers and Trimers. In I_3K dimer simulations, the extended chain geometry still dominates (e.g., BBBH, 9.10%; BBBB, 7.68%; BBBE, 4.02%; EBBB, 2.54%; Figure 5A and Table S1), similar to that in I_3K monomer simulations. Furthermore, the helical population of HHHH decreases significantly to 5.87%. In I_3K trimer simulations, the population of extended chain geometry types increases (e.g., BBBB, 16.11%; BBBH, 11.41%; BBBE, 7.28%; EBBB, 3.97%; BBEB, 3.02%) and the helical population of HHHH decreases further to 4.00% (Figure 5A and Table S1). For L_3K, the helical chain geometry with all α_R conformations, i.e., HHHH, is still dominant in dimer (22.11%) and trimer simulations (20.46%), as shown in Figure 5A and Table S1. There are very few β or extended residue conformations in the top 10 chain geometry types in L_3K dimer simulations, similar to L_3K monomer simulations. In L_3K trimer simulations, the number of chain geometry types with β/extended conformations increases but the population is still small (e.g., BBBB, 1.92%; HBBB, 1.88%; Table S1). Consistent with the chain geometry distributions, the end-to-end distance analysis indicates that the coiled state appears less often and the extended state dominates when more molecules are added to the I_3K system (Figure 5B). For the L_3K dimer and trimer, the coiled state is still dominant, although the extended state appears to be more than that in monomer simulations. I_3K has more chain geometry types with β/extended conformations such as BBBB, which have longer end-to-end distances,

DOI: 10.1021/acs.langmuir.6b00287
Langmuir 2016, 32, 4662−4672

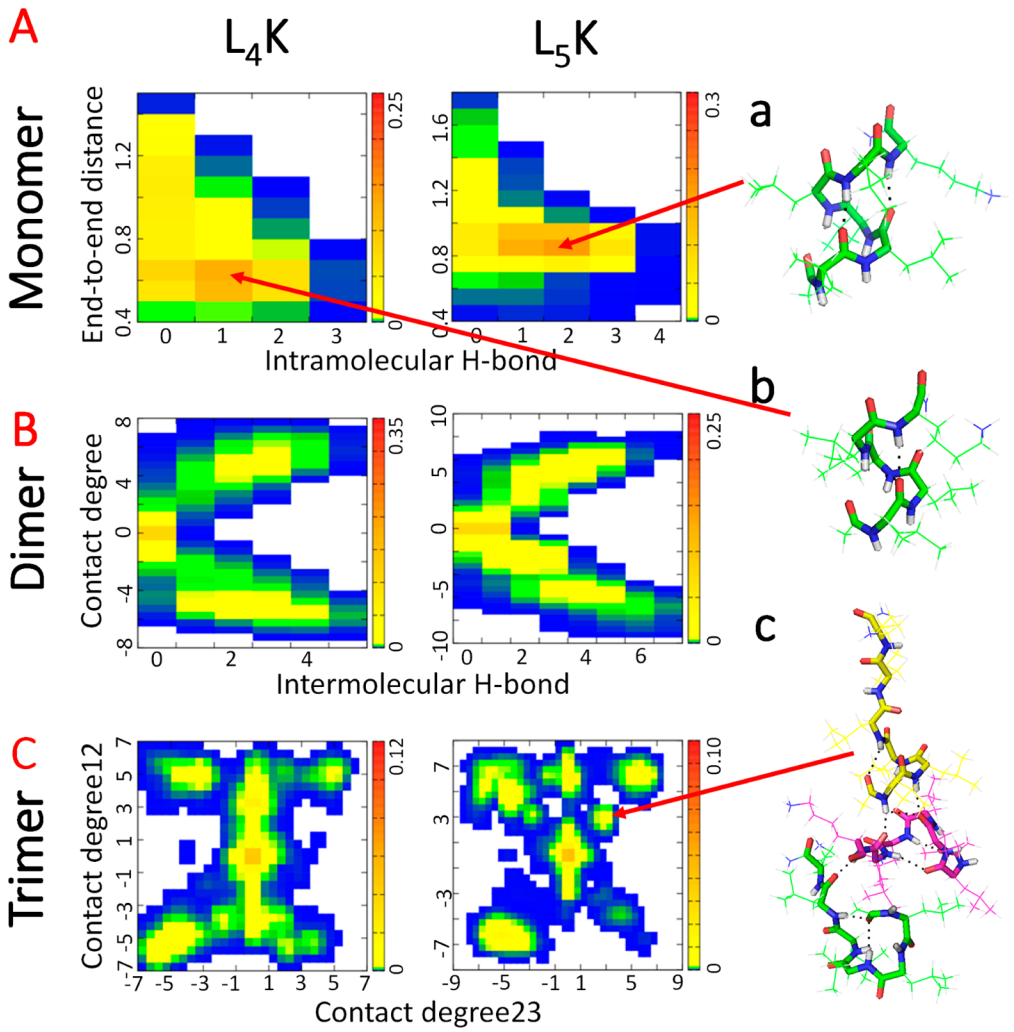

Figure 7. REMD simulation results of monomers, dimers, and trimers of L_4K and L_5K. (A) Probability maps of the end-to-end distances and the intermolecular H-bond numbers of L_4K and L_5K monomers. (B) Probability maps of the contact degree and the intermolecular H-bond number of L_4K and L_5K molecules in dimer simulations. (C) Probability maps of the contact degree of L_4K and L_5K molecules in trimer simulations.

corresponding to the extended state. L_3K has more helical chain geometry types such as HHHH, which have shorter end-to-end distances, corresponding to the coiled state.

3.2.5. Intermolecular and Intramolecular H-Bonding in X_3K Dimers and Trimers. Interbackbone H-bonding is an important intermolecular interaction that favors and stabilizes the alignments of β-strands. Following the above analyses, we then monitor the numbers of both intermolecular and intramolecular H-bonds formed in dimer and trimer simulations. As shown in Figure 6, for I_3K and L_3K dimers, the most populated states contain neither intramolecular nor intermolecular H-bonding. The secondary populated state of the I_3K dimer has two intermolecular H-bonds but no intramolecular H-bonds. The secondary populated state of the L_3K dimer has one intramolecular H-bond but no intermolecular H-bonds. In trimer simulations, both the intermolecular H-bonding of I_3K molecules and the intramolecular H-bonding of L_3K molecules are strengthened, i.e., three to five intermolecular H-bonds and no intramolecular H-bonding in the most populated states of the I_3K trimer; one to two intramolecular H-bonds and one intermolecular H-bond in the most populated states of the L_3K trimer. These results indicate that during microscopic oligomerization, L_3K molecules tend to form more intramolecular H-bonds and fewer intermolecular H-bonds than I_3K.

Although intermolecular interactions in oligomers improve the population of the β/extended conformations of residues and subsequently that of the extended backbones of X_3K peptides, these improvements for L_3K are limited and not large enough to dominate its self-assembly; that is, the self-assembly process of L_3K is still dictated by the intrinsic conformational propensity of Leu residues. As a result, we have observed that L_3K had a poor ability to form β-sheet alignments but I_3K favored β-sheet self-assembly in experiments.[23]

3.3. Effects of Molecular Lengths of L_mK. As indicated above, it is still difficult for L_3K molecules to form stable β-sheet alignments in aggregates. Then, we extend our simulations on L_4K and L_5K molecules in order to reveal the influence of increasing the molecular length. Our previous experiments have indicated a structural transition of L_mK peptides upon increasing the number of hydrophobic residues, i.e., L_5K self-assembled into long nanofibrils with a typical β-sheet structure. The increased intermolecular hydrophobic interactions were proposed to cooperatively enhance the intermolecular H-bonding interactions.[23]

DOI: 10.1021/acs.langmuir.6b00287
Langmuir 2016, 32, 4662−4672

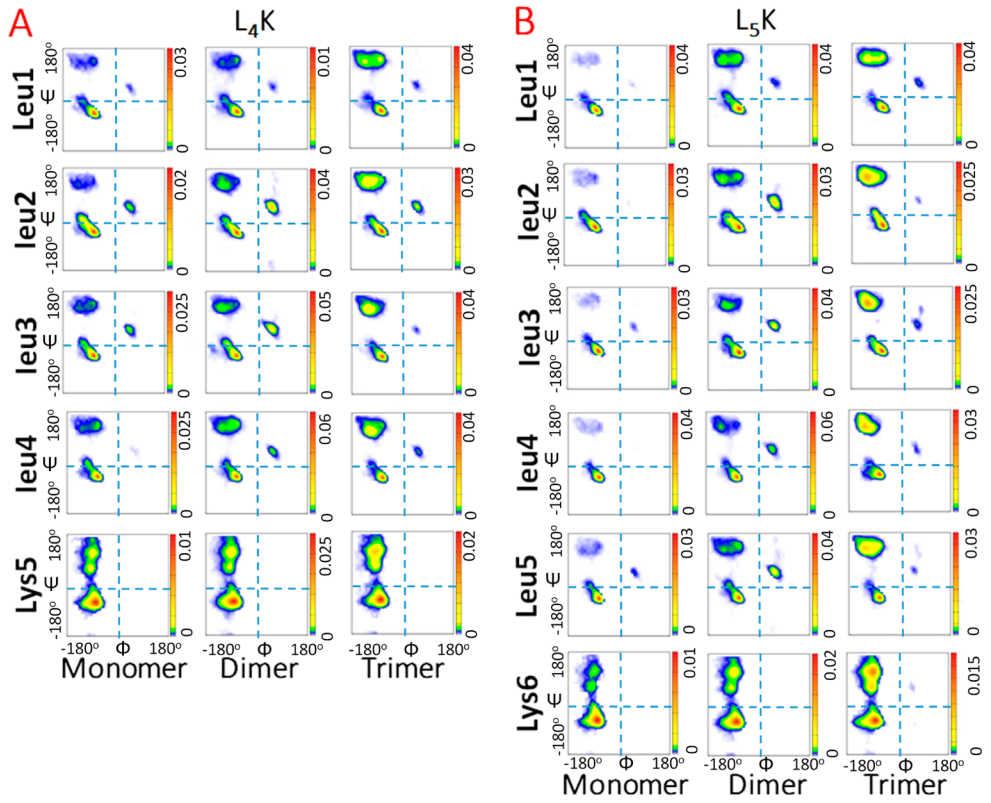

Figure 8. Ramachandran maps for the residues of L_4K and L_5K in dimer and trimer simulations.

3.3.1. Structures of L_mK Monomer, Dimer, and Trimer. As shown in Figure 7A, increasing the length of the hydrophobic part, i.e., the number of hydrophobic residues, favors the formation of intramolecular H-bonds by the L_mK monomer. The most populated structure of the L_4K monomer in the coiled state is an α-helix secondary structure in which the C═O of Leu1 and the N−H of Lys5 form one H-bond (Figure 7A, structure b), in comparison to the most populated structure of the L_3K monomer without intramolecular H-bonding (Figure 1B, structure c). The most populated structure of the L_5K monomer includes two stable intramolecular H-bonds between Leu1 and Leu5 and between Leu2 and Lys6, respectively, which most likely lead to a more stable and complete α-helix structure (Figure 7A, structure a). As shown in Figure 7B and Figure S5, however, the dimer simulations of L_4K and L_5K are similar to that of I_3K rather than L_3K, also revealing three main regions, i.e., dimer aggregates with very limited intermolecular H-bonding (no H-bonding in the case of L_4K, zero and one H-bond in the case of L_5K) and parallel and antiparallel alignments with more intermolecular H-bonds. The results from L_4K trimer simulations are also similar to those from I_3K trimer simulations, in which six main regions are observed, including trimer aggregates without intermolecular H-bonding, parallel and antiparallel dimers, parallel and antiparallel trimers, and mixed trimers of parallel and antiparallel alignments (Figures 7C and S6). Although six regions are also found in the trimer simulations of L_5K, they are slightly different from those of L_4K. There are very few antiparallel dimers but a large population of antiparallel trimers, which implies that the transition from antiparallel dimers to antiparallel trimers is quick and complete. In addition, because the long backbone of L_5K also favors the formation of intramolecular H-bonds, we observe some coiled aggregates with both intramolecular and intermolecular H-bonds (Figure 7, structure c). These results indicate that increasing the hydrophobic length of L_mK peptides favors the formation of intermolecular H-bonding in aggregates.

3.3.2. Intermolecular Interactions Overwhelming the Intrinsic Conformation Preference of Amino Acid Residues. Compared to those of L_3K, Leu residues of L_4K and L_5K in monomer simulations show a decreased probability for β/extended conformations but an increased probability for α_R conformations (Figure 8). When the number of molecules is increased as in dimer and trimer simulations, however, the β/extended populations of Leu residues increase markedly but their α_R populations remain almost unchanged (Figure 8). Furthermore, the increased degrees of β/extended populations are much larger in the L_5K dimer and trimer than in the L_4K dimer and trimer. Such results can be ascribed to the increased interactions between molecules in aggregates (e.g., dimers and trimers), in particular, upon increasing the number of hydrophobic residues. Although the dihedral angle distributions of amino acid residues are generally perceived to depend on their intrinsic preferences for secondary structures, as in the cases of I_3K and L_3K, such a relationship can be significantly altered by increasing the intermolecular interactions, as in the cases of L_4K and L_5K dimers and trimers.

The permutation of residue conformations of a five-residue peptide has 5^5 (3125) types of chain geometry, and a six-residue peptide has 5^6 (15 625) types. As shown in Figurse 5 and S4, similar to the four-residue peptides, not all types of chain geometry can be sampled; furthermore, the convergence toward a few types is more marked in L_4K and L_5K simulations. The helical chain geometry types with α_R conformations (HHHHH and HHHHHH) are still dominant in monomer, dimer, and trimer simulations of L_4K and L_5K. Although only very few β or extended residue conformations are involved in

DOI: 10.1021/acs.langmuir.6b00287
Langmuir 2016, 32, 4662−4672

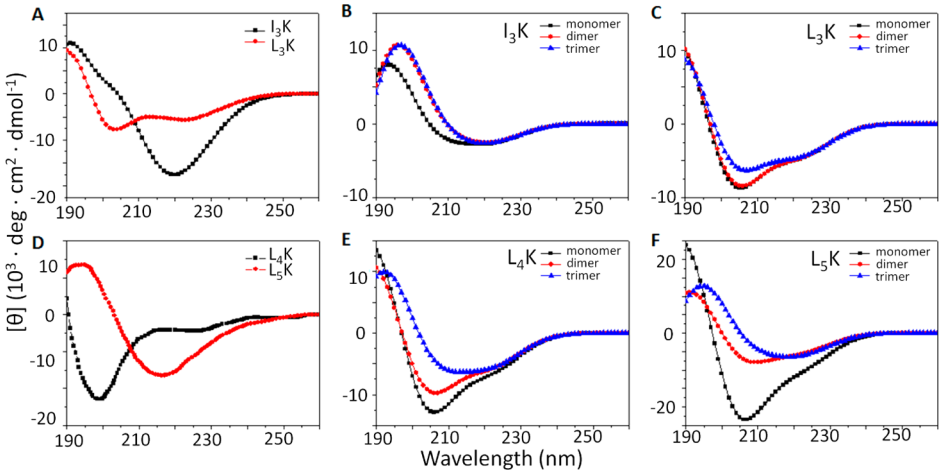

Figure 9. Comparison of experimental and simulated CD spectra. Experimental CD spectra of (A) 8 mM I_3K and 8 mM L_3K at pH 7.0 and (D) 1 mM L_4K and 0.3 mM L_5K at pH 7.0. Simulated CD spectra of (B) I_3K, (C) L_3K, (E) L_4K, and (F) L_5K.

the top 10 chain geometry types in monomer and dimer simulations (Figure S4, Figure 5, and Table S1), chain geometry types with β/extended conformations occur with clearly increased populations in trimer simulations, such as BBBBB of L_4K (6.95%) and BBBBBB of L_5K (8.63%), as shown in Figure 5 and Table S1. These results are consistent with the increased β/extended populations of Leu residues in L_4K and L_5K trimer simulations, as shown in Figure 8.

As shown in Figure 6, the H-bonding number analysis shows the competition between intramolecular and intermolecular H-bonding interactions in the peptide dimers and trimers. As the length and number of molecules are increased, the competition between intermolecular and intramolecular H-bonding is observed to vary. Compared to L_3K, the probability of intermolecular H-bonding increases in the dimer simulations of both L_4K and L_5K and is broadly equivalent to that of intramolecular H-bonding. In trimer simulations, the probability of intermolecular H-bonding of L_5K is even higher than that of intramolecular H-bonding. Generally, the number of intermolecular H-bonds needs to reach a considerable value to stabilize the H-bonding interaction between molecules, but one intramolecular H-bond is enough to stabilize a helical structure.

The end-to-end distance analysis provides information that is complementary to chain geometry and intra/intermolecular H-bonding. Generally, a molecule that adopts an extended backbone in the self-assembled state has a longer end-to-end distance. As shown in Figure S4, the predominance of shorter end-to-end distances in the monomer simulations of L_4K and L_5K is consistent with the formation of coiled states. As shown in Figure 5, the populations of the extended states with longer end-to-end distances increase in the dimer and trimer simulations of L_4K and L_5K. Considering that the extended states of L_4K and L_5K monomers are in much lower populations compared to that of the L_3K monomer (Figure S4), the increase in the populations of the extended states with longer end-to-end distances from monomers to dimers and trimers of L_mK becomes larger upon increasing the number of hydrophobic residues (Figure 5). It should be noted that even for L_5K, the population of the extended states with longer end-to-end distances is still lower than that of I_3K, implying a lower self-assembly efficiency of L_5K relative to that of I_3K. This might explain why fewer nanofibrils were observed in the solution of L_5K in experiments.[23]

These results together indicate that the increased hydrophobic interactions between L_5K molecules can overwhelm the intrinsic conformational propensity of Leu residues and drive the molecules to assemble and form intermolecular H-bonds, finally enhancing the formation of β-strands. The simulation results are thus consistent with our previous study by lending microscopic and mechanistic interpretations to our experimental observations.

3.4. Further Validation Using Simulated and Experimental CD Spectra. Finally, we correlate simulations with experimental observations by comparing CD spectra. The simulated CD spectra are obtained from the converged ensembles of simulations of monomers, dimers, and trimers at 293 K. In spite of being calculated from small numbers of molecules, they show characteristic peaks of typical secondary structures. In experiments, the peptides show characteristic peaks of typical secondary structures only at the concentrations above their critical aggregation concentrations (CACs).

At a concentration of 8 mM, I_3K displays a negative peak at 220 nm, characteristic of β-sheet structures, while L_3K shows two negative peaks at 203 and 223 nm, respectively, which can be ascribed to α-helix structures (Figure 9A). Note that for α-helix structures, H-bonding typically occurs between the C═O of the n residue and the N−H of the n + 4 residue. In the case of L_3K, the H-bonding interaction likely arises from the interaction between the C═O of the acetyl group and the N−H of Lys4, as shown in Figures 2 and 3. In simulations, the I_3K monomer exhibits CD signals that are similar to those of β-sheets (Figure 9B), although no intermolecular H-bonding can be formed in this case. This result implies that the extended backbone of the I_3K monomer has chain geometry that is similar to that of I_3K β-strands in aggregates (Figure 9B). In I_3K dimer and trimer simulations, the characteristic negative peak at 220 nm for β-sheet structures becomes more evident (Figure 9B), which is consistent with the experimental observation (Figure 9A), indicating the formation of intermolecular β-sheet H-bonds. In simulations, the monomer, dimer, and trimer of L_3K all exhibit characteristic α-helix signals (two negative peaks at 206 and 220 nm, Figure 9C), consistent with the experimental observation (Figure 9A). In the L_3K trimer, however, the negative peak at 206 nm appears to be weaker in intensity, which could be ascribed to the slightly increased population of the extended states.

DOI: 10.1021/acs.langmuir.6b00287
Langmuir 2016, 32, 4662−4672

As shown in Figure 9D, L_4K at a concentration of 1.0 mM displays a negative peak at 197 nm, indicating an unordered structure, and L_5K at 0.3 mM shows two characteristic peaks of β-sheets at 198 and 217 nm, respectively. In CD simulations, L_4K and L_5K monomers show stronger negative peaks at 206 and 220 nm than does the L_3K monomer (Figure 9C,E,F), consistent with the conclusion from the above simulations that increasing the number of hydrophobic residues favors the formation of intramolecular H-bonds (Figure 7A). In CD simulations of trimers, however, L_4K exhibits a pattern similar to that of the I_3K monomer (Figure 9E). In the two cases, the negative band is significantly broadened, suggesting the presence of other secondary structures such as α-helices and coils in addition to β-sheets (Figure S6). In fact, CD spectra in both experiments and simulations are a linear combination of CD signals from various secondary structures with distinctly different intensities.[38] Such a phenomenon is reminiscent of the simulated CD spectra of a protein with multiple states.[39] The L_5K trimer exhibits characteristic β-sheet signals, similar to those of the I_3K dimer and trimer (Figure 9B,F). The simulated CD spectra of L_4K and L_5K dimers are intermediate between those of L_4K and L_5K monomers and trimers. Overall, the simulated CD spectra are consistent with the experimental spectra, and their comparison confirms again that the increased hydrophobic interactions favor intermolecular H-bonding and the formation of β-strands.

4. CONCLUSIONS

The self-assembly of short peptides has shown great potential for the creation of novel biomaterials. The relationship between amino acid residues/peptide sequences and self-assembly structures/properties is highly required for mechanistically understanding peptide self-assembly and designing effective self-assembling systems. In the present simulation study on short self-assembling peptides (I_3K, L_3K, L_4K, and L_5K), amino acid residues can retain their intrinsic conformational propensities in some cases but also exhibit conformational features that contradict their intrinsic conformational propensities in other cases. The conformational propensities of amino acid residues are found to be related to their position and adjacent residues in a sequence, the sequence length, and molecular interactions in aggregates.

For X_3K peptides (I_3K and L_3K), the conformational propensities of amino acid residues in the hydrophobic part dictate their aggregating ability and behavior in simulations. I_3K has a stronger propensity to form β-strands as a result of the intrinsic preference of Ile for β-sheet structures, which results in a high probability of forming extended backbones in monomer, dimer, and trimer states. This feature is proposed to favor the formation of intermolecular backbone H-bonding interactions of I_3K and further self-assembly along the H-bonding direction.

Because of the intrinsic propensity of Leu for α-helical structures, L_3K populates mostly coiled structures with significant intramolecular H-bonding in monomer, dimer, and trimer states. The coiled structures disfavor the formation of intermolecular H-bonding between L_3K backbones and prevent further placement of L_3K molecules along the β-sheet H-bonding direction.

When hydrophobic Leu chains are prolonged in L_4K and L_5K, intramolecular interactions become stronger as more intramolecular H-bonds and stable α-helix secondary structures can form in the monomer and intermolecular H-bonding is significantly strengthened in dimer and trimer aggregates. The increased intermolecular interactions in aggregates, particularly the increased hydrophobic interactions with an increasing number of hydrophobic residues, are proposed to drive molecules to assemble and form intermolecular H-bonds, finally resulting in the formation of β-strands and β-sheet alignments. Thus, the intrinsic conformational propensity of Leu residues is not totally successful in the self-assembly of L_mK peptides

By comparing simulated and experimental CD spectra, the above simulation results are further consolidated. Furthermore, the simulation results are consistent with our previous study and provide microscopic and mechanistic interpretations of our experimental observations, i.e., the interplay between the conformational propensity of individual amino acid residue for secondary structures and molecular interactions that determines the self-assembly properties of the peptides and the competition between intramolecular and intermolecular H-bonding interactions that determines the probability of β-sheet alignment of peptide molecules.

■ ASSOCIATED CONTENT

Supporting Information

The Supporting Information is available free of charge on the ACS Publications website at DOI: 10.1021/acs.langmuir.6b00287.

Definition of residue conformations in the Ramachandran map, Ramachandran maps of the X residues in simulations of GGXGG monomers, probability maps of the end-to-end distance and chain geometry type of I_3K and L_3K monomers, chain geometry distributions and end-to-end distances of I_3K, L_3K, L_4K, and L_5K monomers, probability maps of the contact degree and the intermolecular H-bond numbers of L_4K and L_5K in dimer and trimer simulations and representative intermolecular alignments of dimers, and top 10 chain geometry types of I_3K and L_mK monomers, dimers, and trimers simulated at a temperature of 293 K (PDF)

■ AUTHOR INFORMATION

Corresponding Authors

*E-mail: wangyt@itp.ac.cn. Tel: +86-10-62648749.
*E-mail: j.lu.@manchester.ac.uk. Tel: +44-161-3063926.
*E-mail: xuh@upc.edu.cn. Fax: +86-532-86981569. Tel: +86-532-86981569.

Notes

The authors declare no competing financial interest.

■ ACKNOWLEDGMENTS

This work was supported by the National Natural Science Foundation of China under grant nos. 21373270, 11504431, and 11421063. P.Z. acknowledges support from the China Scholarship Council for the study at the University of Washington. Allocations of computer time from SCCAS and the HPC cluster of ITP-CAS are gratefully acknowledged.

■ REFERENCES

(1) Zhang, S. Fabrication of Novel Biomaterials through Molecular Self-Assembly. *Nat. Biotechnol.* **2003**, *21*, 1171−1178.
(2) Ulijn, R. V.; Smith, A. M. Designing Peptide Based Nanomaterials. *Chem. Soc. Rev.* **2008**, *37*, 664−675.

DOI: 10.1021/acs.langmuir.6b00287
Langmuir 2016, 32, 4662−4672

(3) Yan, X.; Zhu, P.; Li, J. Self-Assembly and Application of Diphenylalanine-Based Nanostructures. *Chem. Soc. Rev.* **2010**, *39*, 1877−1890.
(4) Zhao, X.; Pan, F.; Xu, H.; Yaseen, M.; Shan, H.; Hauser, C. A. E.; Zhang, S.; Lu, J. R. Molecular Self-Assembly and Applications of Designer Peptide Amphiphiles. *Chem. Soc. Rev.* **2010**, *39*, 3480−3498.
(5) Reches, M.; Gazit, E. Casting Metal Nanowires within Discrete Self-Assembled Peptide Nanotubes. *Science* **2003**, *300*, 625−627.
(6) Hauser, C. A. E.; Deng, R.; Mishra, A.; Loo, Y.; Khoe, U.; Zhuang, F.; Cheong, D. W.; Accardo, A.; Sullivan, M. B.; Riekel, C.; Ying, J. Y.; Hauser, U. A. Natural Tri- to Hexapeptides Self-Assemble in Water to Amyloid β-Type Fiber Aggregates by Unexpected α-Helical Intermediate Structures. *Proc. Natl. Acad. Sci. U. S. A.* **2011**, *108*, 1361−1366.
(7) Xu, H.; Wang, Y.; Ge, X.; Han, S.; Wang, S.; Zhou, P.; Shan, H.; Zhao, X.; Lu, J. R. Twisted Nanotubes Formed from Ultrashort Amphiphilic Peptide I_3K and Their Templating for the Fabrication of Silica Nanotubes. *Chem. Mater.* **2010**, *22*, 5165−5173.
(8) Chen, P. Self-Assembly of Ionic-Complementary Peptides: A Physicochemical Viewpoint. *Colloids Surf., A* **2005**, *261*, 3−24.
(9) Paramonov, S. E.; Jun, H.-W.; Hartgerink, J. D. Self-Assembly of Peptide-Amphiphile Nanofibers: The Roles of Hydrogen Bonding and Amphiphilic Packing. *J. Am. Chem. Soc.* **2006**, *128*, 7291−7298.
(10) Xu, H.; Wang, J.; Han, S.; Wang, J.; Yu, D.; Zhang, H.; Xia, D.; Zhao, X.; Waigh, T. A.; Lu, J. R. Hydrophobic-Region-Induced Transitions in Self-Assembled Peptide Nanostructures. *Langmuir* **2009**, *25*, 4115−4123.
(11) Chou, P. Y.; Fasman, G. D. Empirical Predictions of Protein Conformation. *Annu. Rev. Biochem.* **1978**, *47*, 251−276.
(12) Schweitzer-Stenner, R. Conformational Propensities and Residual Structures in Unfolded Peptides and Proteins. *Mol. BioSyst.* **2012**, *8*, 122−133.
(13) Oh, K.-I.; Jung, Y.-S.; Hwang, G.-S.; Cho, M. Conformational Distributions of Denatured and Unstructured Proteins Are Similar to Those of 20 × 20 Blocked Dipeptides. *J. Biomol. NMR* **2012**, *53*, 25−41.
(14) Shi, Z.; Chen, K.; Liu, Z.; Ng, A.; Bracken, W. C.; Kallenbach, N. R. Polyproline II Propensities from GGXGG Peptides Reveal an Anticorrelation with β-Sheet Scales. *Proc. Natl. Acad. Sci. U. S. A.* **2005**, *102*, 17964−17968.
(15) Beck, D. A. C.; Alonso, D. O. V.; Inoyama, D.; Daggett, V. The Intrinsic Conformational Propensities of the 20 Naturally Occurring Amino Acids and Reflection of These Propensities in Proteins. *Proc. Natl. Acad. Sci. U. S. A.* **2008**, *105*, 12259−12264.
(16) Oh, K.-I.; Lee, K.-K.; Park, E.-K.; Yoo, D.-G.; Hwang, G.-S.; Cho, M. Circular Dichroism Eigenspectra of Polyproline II and β-Strand Conformers of Trialanine in Water: Singular Value Decomposition Analysis. *Chirality* **2010**, *22*, E186−E201.
(17) Fooks, H. M.; Martin, A. C. R.; Woolfson, D. N.; Sessions, R. B.; Hutchinson, E. G. Amino Acid Pairing Preferences in Parallel β-Sheets in Proteins. *J. Mol. Biol.* **2006**, *356*, 32−44.
(18) Oh, K.-I.; Lee, K.-K.; Park, E.-K.; Jung, Y.; Hwang, G.-S.; Cho, M. A Comprehensive Library of Blocked Dipeptides Reveals Intrinsic Backbone Conformational Propensities of Unfolded Proteins. *Proteins: Struct., Funct., Genet.* **2012**, *80*, 977−990.
(19) Zhong, L.; Johnson, W. C. Environment Affects Amino Acid Preference for Secondary Structure. *Proc. Natl. Acad. Sci. U. S. A.* **1992**, *89*, 4462−4465.
(20) Nyrkova, I.; Semenov, A.; Aggeli, A.; Boden, N. Fibril Stability in Solutions of Twisted-Sheet Peptides: a New Kind of Micellization in Chiral Systems. *Eur. Phys. J. B* **2000**, *17*, 481−497.
(21) Zhou, P.; Deng, L.; Wang, Y.; Lu, J. R.; Xu, H. Different Nanostructures Caused by Competition of Intra- and Inter-β-Sheet Interactions in Hierarchical Self-Assembly of Short Peptides. *J. Colloid Interface Sci.* **2016**, *464*, 219−228.
(22) DeGrado, W. F.; Lear, J. D. Induction of Peptide Conformation at Apolar Water Interfaces. 1. A Study with Model Peptides of Defined Hydrophobic Periodicity. *J. Am. Chem. Soc.* **1985**, *107*, 7684−7689.
(23) Han, S.; Cao, S.; Wang, Y.; Wang, J.; Xia, D.; Xu, H.; Zhao, X.; Lu, J. R. Self-Assembly of Short Peptide Amphiphiles: The Cooperative Effect of Hydrophobic Interaction and Hydrogen Bonding. *Chem. - Eur. J.* **2011**, *17*, 13095−13102.
(24) Aggeli, A.; Nyrkova, I. A.; Bell, M.; Harding, R.; Carrick, L.; McLeish, T. C. B.; Semenov, A. N.; Boden, N. Hierarchical Self-Assembly of Chiral Rod-Like Molecules as a Model for Peptide β-Sheet Tapes, Ribbons, Fibrils, and Fibers. *Proc. Natl. Acad. Sci. U. S. A.* **2001**, *98*, 11857−11862.
(25) López de la Paz, M.; de Mori, G. M. S.; Serrano, L.; Colombo, G. Sequence Dependence of Amyloid Fibril Formation: Insights from Molecular Dynamics Simulations. *J. Mol. Biol.* **2005**, *349*, 583−596.
(26) López de la Paz, M.; Goldie, K.; Zurdo, J.; Lacroix, E.; Dobson, C. M.; Hoenger, A.; Serrano, L. *De novo* Designed Peptide-Based Amyloid Fibrils. *Proc. Natl. Acad. Sci. U. S. A.* **2002**, *99*, 16052−16057.
(27) Boyle, A. L.; Woolfson, D. N. *De novo* Designed Peptides for Biological Applications. *Chem. Soc. Rev.* **2011**, *40*, 4295−4306.
(28) Van Der Spoel, D.; Lindahl, E.; Hess, B.; Groenhof, G.; Mark, A.; Berendsen, H. GROMACS: Fast, Flexible, and Free. *J. Comput. Chem.* **2005**, *26*, 1701−1718.
(29) Brooks, B. R.; Bruccoleri, R. E.; Olafson, B. D.; States, D. J.; Swaminathan, S.; Karplus, M. CHARMM: A Program for Macromolecular Energy, Minimization, and Dynamics Calculations. *J. Comput. Chem.* **1983**, *4*, 187−217.
(30) Darden, T.; York, D.; Pedersen, L. Particle Mesh Ewald: An N* log (N) Method for Computing Ewald Sums. *J. Chem. Phys.* **1993**, *98*, 10089−10092.
(31) Deng, L.; Zhou, P.; Zhao, Y.; Wang, Y.; Xu, H. Molecular Origin of the Self-Assembled Morphological Difference Caused by Varying the Order of Charged Residues in Short Peptides. *J. Phys. Chem. B* **2014**, *118*, 12501−12510.
(32) Bulheller, B. M.; Hirst, J. D. DichroCalc—Circular and Linear Dichroism Online. *Bioinformatics* **2009**, *25*, 539−540.
(33) Oakley, M. T.; Hirst, J. D. Charge-Transfer Transitions in Protein Circular Dichroism Calculations. *J. Am. Chem. Soc.* **2006**, *128*, 12414−12415.
(34) Sugita, Y.; Okamoto, Y. Replica-Exchange Molecular Dynamics Method for Protein Folding. *Chem. Phys. Lett.* **1999**, *314*, 141−151.
(35) Okabe, T.; Kawata, M.; Okamoto, Y.; Mikami, M. Replica-Exchange Monte Carlo Method for the Isobaric-Isothermal Ensemble. *Chem. Phys. Lett.* **2001**, *335*, 435−439.
(36) Hansmann, U. H. E. Parallel Tempering Algorithm for Conformational Studies of Biological Molecules. *Chem. Phys. Lett.* **1997**, *281*, 140−150.
(37) Gnanakaran, S.; Nussinov, R.; Garcia, A. E. Atomic-Level Description of Amyloid β-Dimer Formation. *J. Am. Chem. Soc.* **2006**, *128*, 2158−2159.
(38) Greenfield, N. J. Using Circular Dichroism Spectra to Estimate Protein Secondary Structure. *Nat. Protoc.* **2007**, *1*, 2876−2890.
(39) Ceballos, J. A.; Giraldo, M. A.; Cossio, P. Effects of a Disulfide Bridge Prior to Amyloid Formation of the ABRI Peptide. *RSC Adv.* **2014**, *4*, 36923−36928.

DOI: 10.1021/acs.langmuir.6b00287
Langmuir 2016, 32, 4662−4672